Steering a 3D Limit-Cycle Walker for Collaboration with a Leader

Mohamad Shafiee Motahar, Sushant Veer, and Ioannis Poulakakis

Abstract— **This paper presents a control method for steering three dimensional (3D) dynamically walking bipeds that are engaged in cooperative tasks such as object transportation. Towards achieving safe interaction with a leading human (or robot) collaborator, the walking biped is required to exhibit compliance at the port of interaction, while simultaneously adapting its walking pattern in response to the perceived interaction forces. To address these issues, we propose a method that fuses impedance control of the biped's arm with position control of its legs in a way that the biped adaptively modifies its stepping pattern according to the collaborator's intentions. The method is applied on a 3D bipedal robot that is driven in the workspace by a collaborator, whose intention is communicated to the biped through the interaction force.**

I. Introduction

There is an increasing demand for assistive bipedal robots that are capable of physical interaction with other agents – possibly humans – to accomplish collaborative tasks, such as coordinated object transportation. In such collaborative scenarios, we can rely on the environment mapping and path planning skills of the leading collaborator to choose an obstacle-free trajectory for the team. This intended trajectory may not be directly accessible by the robot; however, the interaction forces developed between the robot and the collaborator offer cues on how the robot should adapt its behavior to accomplish the task. The objective of this paper is to provide a method for gait adaptation of a three-dimensional (3D) limit-cycle biped that allows a collaborator to effectively "walk" the biped along a desired path.

There has been substantial research on cooperative tasks with legged robots; these efforts focus primarily on humanoids walking under the Zero Moment Point (ZMP) criterion of stability. For instance, [1] presents an interaction interface that enables a human to drive the humanoid NAO by applying a force on its hand. The method is based on adjusting heading angle, step length and frequency according to the interaction forces that convey the human's intention. A comprehensive compilation of examples where humanoid robots accomplish manipulation tasks that require locomotion adaptation can be found in the book [2]. However, such tasks have not been explored in dynamically[1] walking bipeds. Indeed, the vast majority of the literature on dynamic bipeds focuses on the realization of stable and robust limit-cycle walking gaits. Relevant methods include, for example, geometric reduction [3], hunting for virtual constraints [4], and hybrid zero dynamics (HZD) [5], [6]. Systematic approaches have also been developed to enhance the robustness of the resulting gaits to modeling uncertainties [7], and to rough terrain [8], [9].

With the intention to engage limit-cycle walkers in tasks that involve their arms, dynamic locomotion controllers have been extended to incorporate manipulation in fully actuated bipeds [10]. In this case, the control system is designed so that the walking gait remains unaffected by the manipulation task, which is effectively planned in the nullspace of the locomotion controller. However, for cooperative tasks – such as coordinated object transportation – interaction forces developed between the robot's arms and the external collaborator may carry important information about the task; thus, these forces may act as command signals that the biped needs to adapt to. Along these lines, the authors' previous work [11]–[13] explored the use of interaction forces for adaption of the biped's speed in planar settings. The purpose of this paper is to extend gait adaptation to 3D limit-cycle walkers, which can adjust not only their speed but also their direction in response to interaction forces.

Dynamic bipedal walking in 3D environments cluttered by obstacles has been explored in a few studies. For example, an event-based controller within the HZD framework was developed in [14] to steer a 3D biped along a desired path with mild curvature. A motion planning framework that composes limit-cycle gait primitives to navigate a 3D dynamic biped amidst obstacles was proposed in [15], [16]. Analytical guarantees for stable execution of such motion plans were offered in [16], while [17] further extended these methods to obtain plans that can be executed with virtually zero drift. All these efforts require the biped to follow a suggested path in the absence of interaction forces.

By way of contrast, this paper proposes a method for navigating limit-cycle walkers in 3D environments by actively modifying their speed and heading angle in response to interaction forces. Our approach is particularly suitable for leader-follower cooperative tasks, in which the biped's manipulator interacts with a leading collaborator in a way that its motion is guided by the collaborator's intentions. This way, the biped can leverage the leader's knowledge regarding the environment and the task. The proposed method relies on integrating impedance control to regulate interaction, with HZD control to synchronize the actuated degrees of freedom (DOF) so that the generated walking gaits can be adapted to external activity. The feasibility of the method is illustrated on a 3D biped that tracks the intended trajectory of a leader in an environment with obstacles *without* any explicit knowledge of the leader's intentions or the environment.

M. S. Motahar, S. Veer and I. Poulakakis are with the Department of Mechanical Engineering, University of Delaware, Newark, DE 19716, USA; e-mail: {motahar, veer, poulakas}@udel.edu.

This work is supported in part by NSF grant NRI-1327614.

[1]Here, the term "dynamically walking" refers to limit-cycle walkers.

II. Walking under Interaction Forces

We consider a fairly generic model of a 3D bipedal walker as shown in Fig. 1. The model is composed of a torso and two identical legs, each connected to the torso via a two-DOF revolute hip joint. The legs are composed of two links – the thigh and the shin – which are connected through a one-DOF revolute knee joint. The biped is equipped with a two-link manipulator that is attached to the torso through a two-DOF revolute shoulder joint. The manipulator enables the biped to interact with its environment via external forces exerted at its end effector as in Fig. 1. We assume that the stance foot acts as a pivot with three rotational DOFs corresponding to the yaw q_1, pitch q_2, and roll q_3 angles; see Fig. 1. During the single support phase, the model has twelve degrees of freedom $q := (q_1, ..., q_{12}) \in \mathcal{Q}$, where $\mathcal{Q}$ contains physically reasonable configurations of the system. Seven actuators – four located at the hip joints, two at the knee joints and one at the roll joint of the foot – provide the input torques for the locomotion system, and three actuators – two at the shoulder joint and one at the elbow joint – provide the input torques for the manipulation system.

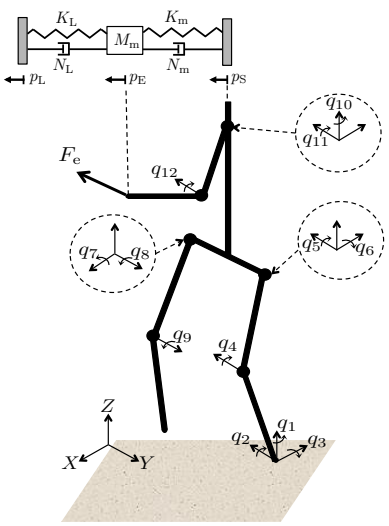

Fig. 1. Robot model with a choice of generalized coordinates and impedance model of interaction.

A. Cooperation Model

Consider a scenario in which the biped-leader team cooperatively transports an object over a distance that requires the locomotion system of the biped to be engaged. The leader's role is to plan an obstacle-free path and guide the biped to follow it by applying a suitable force at the biped's end effector. We assume that the intention of the leading coworker is encoded in a sufficiently smooth trajectory $\mathrm{p_L}(t)$, which is unknown to the biped. Rather, the biped "perceives" the leader's intentions through an interaction force $F_{\mathrm{e}}(t)$ applied at its end effector. Let

$$y_{\mathrm{L}} = h_{\mathrm{L}}(t) := \mathrm{p_L}(t) - \mathrm{p_E}(q(t)) \ . \tag{1}$$

be the tracking error between the end effector location $\mathrm{p_E}(q)$ and the intended location of the leader $\mathrm{p_L}(t)$. As in [18], an impedance model is implemented to translate the leader's intended trajectory to an interaction force[2]; i.e.,

$$F_{\mathrm{e}} = K_{\mathrm{L}} y_{\mathrm{L}} + N_{\mathrm{L}} \dot{y}_{\mathrm{L}} \ , \tag{2}$$

where K_{L} and N_{L} are the corresponding stiffness and damping matrices; see Fig. 1. Note that (2) incorporates the leader's response to the robot's activity; if the biped follows the intention of leader closely, the leader applies a smaller force on biped's end effector.

B. Walking Model

Due to the nontrivial length of the hip joint, the equations of motion during the left and right leg support phases are different. In what follows, we develop a model for the left leg support phase; the equations for the right leg can be derived in a similar manner. The dynamics of the biped in the swing phase can be written as

$$D(q)\ddot{q} + C(q,\dot{q})\dot{q} + G(q) = B_\ell u_\ell + B_{\mathrm{m}} u_{\mathrm{m}} + J_{\mathrm{E}}^{\mathrm{T}}(q) F_{\mathrm{e}}, \tag{3}$$

where $D(q)$ is the mass matrix, $C(q,\dot{q})\dot{q}$ contains the centrifugal and Coriolis forces and $G(q)$ contains the gravitational forces. The matrices B_ℓ and B_{m} distribute the locomotion inputs u_ℓ and manipulation inputs u_{m} to the configuration variables q. Finally, $J_{\mathrm{E}}(q) := \partial \mathrm{p_E}(q)/\partial q$, where $\mathrm{p_E}$ is the position of biped's end-effector, at which the interaction force F_{e} is applied; see Fig. 1. Defining the state vector $x := (q^{\mathrm{T}}, \dot{q}^{\mathrm{T}})^{\mathrm{T}}$, the swing phase dynamics (3) can be written in state-space form

$$\dot{x} := f(x) + g_\ell(x) u_\ell + g_{\mathrm{m}}(x) u_{\mathrm{m}} + g_{\mathrm{e}}(x) F_{\mathrm{e}} \ , \tag{4}$$

where $x \in T\mathcal{Q} := \left\{(q,\dot{q}) \mid q \in \mathcal{Q},\ \dot{q} \in \mathbb{R}^{12}\right\}$ and the vector fields f, g_ℓ, g_{m}, g_{e} are defined accordingly.

Single support proceeds until the swing toe impacts the ground in front of the stance leg; i.e., when the solution of (4) intersects the surface

$$\mathcal{S} := \{(q,\dot{q}) \in TQ \mid p_{\mathrm{v}}(q) = 0,\ \dot{p}_{\mathrm{v}}(q,\dot{q}) < 0\} \ , \tag{5}$$

where p_{v} denotes the height of the swing leg.

When the swing toe contacts the ground, double support is initiated. As in [5, Section 3.4.2], we assume that double support is instantaneous and that no rebound or slip occurs at the impact. The double support phase can be described by a map $\Delta : \mathcal{S} \to T\mathcal{Q}$ taking the pre-impact state $x^- \in \mathcal{S}$ to the post-impact state $x^+ \in T\mathcal{Q}$ that provides an initial condition for the subsequent swing phase; i.e.

$$x^+ = \Delta(x^-) \ . \tag{6}$$

The derivation of Δ is skipped here for brevity. The reader can find the details in [6].

Combining the swing and impact phases, the model can be expressed in the form of a system with impulse effects as

$$\Sigma : \begin{cases} \dot{x} = f(x) + g_\ell(x) u_\ell + g_{\mathrm{m}}(x) u_{\mathrm{m}} + g_{\mathrm{e}}(x) F_{\mathrm{e}}, & x^- \notin \mathcal{S}, \\ x^+ = \Delta(x^-), & x^- \in \mathcal{S}, \end{cases}$$

where the symbols have the meaning explained above.

[2]In experimental implementation, the force $F_{\mathrm{e}}(t)$ should be known via a force sensor.

III. Coupled Locomotion and Arm Control

This section develops a control law that regulates the arm's impedance in response to the external force, while generating walking gaits through an HZD-based controller.

A. Virtual Constraints for the Locomotion Task

Walking is realized by assigning output functions in the form of virtual holonomic constraints to the actuated joints of the legs with the control objective being to drive these outputs to zero. Consider the output function

$$\hat{y}_\ell = \hat{h}_\ell(q) := q_{\rm a} - h_\ell^{\rm des}(\theta(q)) \ , \tag{7}$$

where $q_{\rm a} := (q_3, \dots, q_9)$ includes the controlled variables of the legs and $h_\ell^{\rm des}$ denotes the desired evolution of these variables as a function of the quantity $\theta(q) = -q_2 - q_4/2$, which corresponds to the angle of the line connecting the foot of the support leg with the corresponding hip joint. The function $h_\ell^{\rm des}$ is designed using Beziér polynomials of degree equal to three as detailed in [11].

In general, there is no guarantee that the output (7) remains zero under the effect of the impact map Δ of (6). To achieve this we follow a technique detailed in [6], according to which (7) is augmented with a correction term $h_{\rm c}(\theta, \beta)$ as

$$y_\ell = h_\ell(q, \beta) := q_{\rm a} - h_\ell^{\rm des}(\theta) - h_{\rm c}(\theta, \beta) \ . \tag{8}$$

The correction output $h_{\rm c}$ is chosen to be a three times continuously differentiable piecewise polynomial function of θ. The vector of coefficients β is updated on a step-to-step basis so that the initial error with respect to the (uncorrected) output (7) is smoothly rejected by the middle of the step; see [6] for more details.

B. Impedance Regulation for the Manipulation Task

The manipulation task is encoded in a set of suitably designed output functions, the purpose of which is to regulate the configuration of the arm. Consider

$$y_{\rm m} = h_{\rm m}(q) := p_{\rm E}(q_{\rm m}) - h_{\rm m}^{\rm des}(\theta(q)) \ , \tag{9}$$

where $p_{\rm E}$ is the position of the end effector with respect to a local frame attached to the shoulder, $q_{\rm m} := (q_{10}, q_{11}, q_{12})$ contains the configuration variables of the arm. The desired evolution $h_{\rm m}^{\rm des}(\theta(q))$ is a vector of degree three Beziér polynomials that describes the desired position of end effector relative to the shoulder joint; equivalently, $h_{\rm m}^{\rm des}(\theta(q))$ can be viewed as the desired configuration of the arm. The goal of the impedance controller is to enforce a mechanical impedance relation that governs the evolution of the output (9) in response to the interaction force $F_{\rm e}$; that is,

$$M_{\rm m}\ddot{y}_{\rm m} + \frac{N_{\rm m}}{\epsilon_{\rm m}}\dot{y}_{\rm m} + \frac{K_{\rm m}}{{\epsilon_{\rm m}}^2}y_{\rm m} = F_{\rm e} \ , \tag{10}$$

where $\epsilon_{\rm m} > 0$ is a parameter, and $M_{\rm m}$, $N_{\rm m}$, and $K_{\rm m}$ are positive definite mass, damping and stiffness matrices, respectively, determining the compliance of the arm. In the absence of an external force, (10) implies that the error $y_{\rm m}$ converges to zero at a rate specified by the matrices $M_{\rm m}$, $N_{\rm m}$, and $K_{\rm m}$ and the parameter $\epsilon_{\rm m}$, so that the arm settles at its desired configuration captured by $h_{\rm m}^{\rm des}$.

C. Controller Design

The objective of the controller is to drive the locomotion outputs (8) to zero and to establish the desired mechanical impedance relationship (10). To achieve this, the outputs (8) and (9) are augmented in a single output vector and differentiated to expose the input/output relation

$$\begin{bmatrix} \ddot{y}_\ell \\ \ddot{y}_{\rm m} \end{bmatrix} = L_f^2 h(x) + L_g L_f h(x) \begin{bmatrix} u_\ell \\ u_{\rm m} \end{bmatrix} + L_{g_{\rm e}} L_f h(x) F_{\rm e} \ , \tag{11}$$

where $h(x) := (h_\ell^{\rm T}(x), h_{\rm m}^{\rm T}(x))^{\rm T}$, $g(x) := (g_\ell(x), g_{\rm m}(x))$, and $L_f^2 h$, $L_g L_f h$ and $L_{g_{\rm e}} L_f h$ denote the Lie derivatives of h along the corresponding vector fields; see [5, Section B.1.5] for relevant definitions. Under the condition that the decoupling matrix $L_g L_f h$ is invertible and assuming that the external force can be measured, the control law

$$\begin{bmatrix} u_\ell \\ u_{\rm m} \end{bmatrix} = L_g L_f h(x)^{-1} \left(\begin{bmatrix} v_\ell(y_\ell, \dot{y}_\ell) \\ v_{\rm m}(y_{\rm m}, \dot{y}_{\rm m}, F_{\rm e}) \end{bmatrix} - L_f^2 h(x) - L_{g_{\rm e}} L_f h(x) F_{\rm e} \right) \tag{12}$$

leads to the linear input/output relation

$$\begin{bmatrix} \ddot{y}_\ell \\ \ddot{y}_{\rm m} \end{bmatrix} = \begin{bmatrix} v_\ell(y_\ell, \dot{y}_\ell) \\ v_{\rm m}(y_{\rm m}, \dot{y}_{\rm m}, F_{\rm e}) \end{bmatrix} \ , \tag{13}$$

where v_ℓ and $v_{\rm m}$ are auxiliary control variables. Selecting

$$v_\ell(y_\ell, \dot{y}_\ell) = -\frac{1}{\epsilon_\ell} N_\ell \dot{y}_\ell - \frac{1}{\epsilon_\ell^2} K_\ell y_\ell \tag{14}$$

ensures that the output y_ℓ converges to zero at a rate dependent on the positive definite matrices K_ℓ, N_ℓ and the positive parameter ϵ_ℓ. Furthermore, choosing

$$v_{\rm m}(y_{\rm m}, \dot{y}_{\rm m}, F_{\rm e}) = M_{\rm m}^{-1}(F_{\rm e} - \frac{N_{\rm m}}{\epsilon_{\rm m}}\dot{y}_{\rm m} - \frac{K_{\rm m}}{\epsilon_{\rm m}^2} y_{\rm m}) \tag{15}$$

results in the desired impedance relationship (10). The system Σ in closed loop with the control law (12) becomes

$$\Sigma_{\rm cl}: \begin{cases} \dot{x} = f_{\rm cl}^\beta(x) + g_{\rm cl}^\beta(x) F_{\rm e}, & x \notin \mathcal{S}, \\ x^+ = \Delta(x^-), & x^- \in \mathcal{S}, \end{cases} \tag{16}$$

where $f_{\rm cl}^\beta$, $g_{\rm e,cl}^\beta$ are defined accordingly. Note that these vector fields depend on the parameter β of the correction term $h_{\rm c}$ of (8) that is updated at the beginning of each step.

IV. Effect of External Force on Locomotion

This section discusses certain key properties of the closed-loop system (16) that are important in realizing adaptable locomotion in the presence of the interaction force.

A. Effect of External Force on Stepping Pattern

An important property of the controller of Section III is that the step length and step width of the biped are *not* affected by the external force. To see this, let $q_\ell := (q_2, \cdots, q_9)$ denote the configuration of the legs excluding the yaw angle q_1. The locomotion output h_ℓ in (8) and the height $p_{\rm v}$ of the swing leg in (5) depend *only* on q_ℓ.

Since the correction output in (8) accounts for the induced initial error by the interaction force and rejects it before the robot completes a step, the solution of the equation $(h_\ell(q_\ell^-,\beta), p_{\rm v}(q_\ell^-)) = (\dot{h}_\ell(q_\ell^-), p_{\rm v}(q_\ell^-)) = (0,0)$ uniquely determines the locomotion configuration q_ℓ^- prior to impact. As a result, the step length, step width and θ^- which solely depend on q_ℓ^-, remain constant over different steps. The importance of this observation lies in the fact that, as will be shown in Section V, the adaptation mechanism that allows the biped to follow the leader's intention effectively modifies the biped's stride frequency and heading direction.

B. Effect of External Force on Symmetry under Yaw Rotation

A second property that is important – particularly in steering – is the symmetry of the unforced Poincaré map with respect to yaw rotations and the associated symmetry breaking upon the application of an external force at the biped's end effector.

Consider the case where no external force is applied. The unforced Poincaré map $P : \mathcal{S} \to \mathcal{S}$ transfers the state $x[k]$ at the k-th step one step ahead; i.e.

$$x[k+1] = P(x[k]) \ . \tag{17}$$

Since the control law (12) does *not* depend on the yaw angle q_1, [16, Proposition 1] implies that P can be decomposed as

$$P(x) = \begin{bmatrix} q_1 + P^{(q_1)}(\tilde{x}) \\ \tilde{P}(\tilde{x}) \end{bmatrix} \ , \tag{18}$$

where $\tilde{x}$ is the projection of x to its non-q_1 part, i.e. $\tilde{x} := (x_2, \dots, x_{18})$, and $P^{(q_1)}$ and $\tilde{P}$ are defined as in the proof of [16, Proposition 1]. Equation (18) implies that the unforced Poincaré map is equivariant[3] under yaw rotations. In words, if we perturb the nominal heading angle q_1^* by an amount δq_1, the biped will continue taking steps along the new heading direction $q_1^* + \delta q_1$.

It is important to emphasize that the presence of the external force $F_{\rm e}$ breaks the symmetry discussed above. This is because the term $J_{\rm E}(q)$ in (3) depends on the yaw angle q_1. As a result, the application of $F_{\rm e}$ can be used to induce turning on the biped, enabling the leader to change the heading angle of the biped to a new desired one by applying a suitable force. Note that once the biped settles at the desired direction, then the external force is no longer required to maintain the new direction. It should be mentioned here that a similar conclusion does not hold for the case where the leader wants to change the biped's speed, which depends on $\tilde{x}$. In this case, the leader needs to keep applying a force to maintain the desired speed, since if the force is removed, the exponential stability of the fixed point $\tilde{x}^*$ of $\tilde{P}$ will bring the speed of the biped back to its nominal unforced value.

C. Effect of External Force on Zero Dynamics

This section provides insight about the response of the biped to external forces by studying the zero dynamics. The control law (12) renders the zero dynamics surface

$$\mathcal{Z} := \{x \in TQ \mid h_\ell(q,\beta) = 0, \ L_{f_{\rm cl}} h_\ell(x,\beta) = 0\}$$

attractive and invariant under the flow of the swing phase dynamics and the impact map. Note that unlike the planar case considered in [11], the motion of biped's arm due to impedance dynamics (10) does not break the hybrid invariance of $\mathcal{Z}$; for, the correction output $h_{\rm c}$ accounts for any initial error in the locomotion output (7) induced by the arm's motion, and rejects it before the next impact occurs. As a result, a five-DOF *Forced Hybrid Zero Dynamics (FHZD)* emerges from the closed loop dynamics (16). The FHZD is

$$\Sigma_{\rm z} : \begin{cases} \dot{z} = f_{\rm z}^\beta(z) + g_{\rm z}^\beta(z) F_{\rm e}, & z \notin \mathcal{S} \cap \mathcal{Z} \\ z^+ = \Delta_{\rm z}(z^-), & z^- \in \mathcal{S} \cap \mathcal{Z} \end{cases} \ , \tag{19}$$

where $z := (q_z^{\rm T}, \dot{q}_z^{\rm T})^{\rm T}$ with $q_{\rm z} := (q_1, \theta, q_{10}, q_{11}, q_{12})$ being a valid set of coordinates on $\mathcal{Z}$. In (19), $f_{\rm z}^\beta := f_{\rm cl}^\beta|_{\mathcal{Z}}$ and $g_{\rm z}^\beta := g_{\rm cl}^\beta|_{\mathcal{Z}}$ are the restrictions on $\mathcal{Z}$ of the closed loop dynamics (16), and $\Delta_{\rm z} := \Delta|_{\mathcal{S}\cap\mathcal{Z}}$. The explicit form of the continuous-time part of the FHZD in (19) can be derived in a similar manner as described in [6, Section III], with the additional step of including the desired impedance dynamics (10) in the zero dynamics. The details are provided in the Appendix.

The FHZD (19) has important implications in a cooperation scenario. First, it is clearly seen from (19) that the evolution of the unactuated DOFs q_1 and θ are affected by the external force. Physically, this means that the biped changes its heading angle as well as its speed in response to the external force. Second, the dynamics of q_1 and θ in (19) are coupled, implying that a speed change in the direction of motion of the biped can change the heading angle as well. The choice of locomotion and manipulation outputs play an important role in the dynamics of (19) and influences this coupling behavior; see (27) in the Appendix. Therefore, if a desired response to the external force is sought, one can design the outputs accordingly; this topic will be further discussed in Section V. Third, in the absence of perturbations, the evolution of the biped can be obtained by integration of the reduced system (19), significantly reducing the computational time compared to integrating the full-order system (16).

V. 3D Steering to a Goal Region via Interaction

In this section, details regarding the implementation of the controller are discussed and the method is evaluated in simulation to steer a 3D biped amidst obstacles in a collaborative task.

A. Implementation Aspects

We begin by computing unforced walking motions by numerically searching for suitable fixed points of the Poincaré map (17) that satisfy

$$x^* = P(x^*) \ . \tag{20}$$

Beyond the periodicity constraint (20), additional constraints related to actuator saturation, foot-ground clearance and

[3]Mathematically, if $\Psi_g(x) = (q_1 + g, \ \tilde{x}^{\rm T})^{\rm T}$, then $P \circ \Psi_g = \Psi_g \circ P$.

interaction, and other practical considerations similar to [5, Section 3.2] can be incorporated in the optimization.

The existence of an external force applied at the end effector calls for additional specifications to be considered when computing unforced periodic motions. For example, we have computed unforced periodic gaits that are symmetric with respect to the X-axis; see Fig. 1. However, upon application of an external force $F_{\mathrm{e,x}}$ acting *only* along the X-axis, the overall motion of the biped deviates from the X-direction. This is not surprising as $F_{\mathrm{e,x}}$ affects the dynamics of the heading angle q_1 despite the fact that it is perfectly aligned with the direction of the unforced motion; this is evident by (27) in the Appendix. Clearly, this behavior is undesirable in a cooperation task. It implies that if the leader intends to accelerate or decelerate the biped along the direction of motion, it will also need to apply excessive forces in the Y direction to keep the biped walking straight. To reduce the effect of $F_{\mathrm{e,x}}$ on heading we consider the cost function

$$\Big|\frac{\partial P^{(q_1)}(x)}{\partial F_{\mathrm{e,x}}}\Big|_{x=x^*}, \tag{21}$$

in the optimization process associated with the computation of fixed points; in (21), $P^{(q_1)}(x)$ is the map defined in (17). This way, the resulting periodic orbits exhibit smaller deviations from the nominal direction when an external force is applied.

B. Evaluation in Simulation

We now consider a scenario in which a leading collaborator – possibly a human – intends to move an object with the help of a bipedal robot to a desired location in the workspace of Fig. 2(a). The leader plans an obstacle-free trajectory $p_{\mathrm{L}}(t)$ for the object so that all the specifications of the task are fulfilled. The biped needs to adapt its motion to the leader's intended trajectory, the explicit form of which is unknown. However, it turns out that the interaction force developed as a result of the leader's intentions can provide sufficient information to steer the biped accordingly. In the numerical implementation of this scenario, the impedance parameters of the leader are selected to be $K_{\mathrm{L}} = 10\mathrm{N/m}$ and $N_{\mathrm{L}} = 2\mathrm{Ns/m}$, and the parameters of the arm impedance controller are chosen as $M_{\mathrm{m}} = I_{3\times3}\mathrm{Kg}$, $K_{\mathrm{m}} = 20I_{3\times3}\mathrm{N/m}$, $N_{\mathrm{m}} = 4I_{3\times3}\mathrm{Ns/m}$, where $I_{3\times3}$ is the 3×3 identity matrix, and $\epsilon_{\mathrm{m}} = 0.5$. In the simulations that follow, care is taken so that actuator saturation and friction cone limitations are respected throughout the motion of the biped.

Figures 2(b) and 2(c) present the interaction force and average speeds of the biped and the leader, respectively. As expected, the biped perceives the leader's acceleration as an increase in the X component of the force, and its left turning as an increase in the Y component; see Fig. 2(b). As the biped turns, its average speed converges to that of the leader, as shown in Fig. 2(c). After the narrow passage between the two obstacles of Fig. 2(a), the biped is guided to walk with the same speed and direction it started. As a result, the biped converges to a new forced limit cycle that is almost identical to the unforced one, as Fig. 2(d) and 2(e) show.

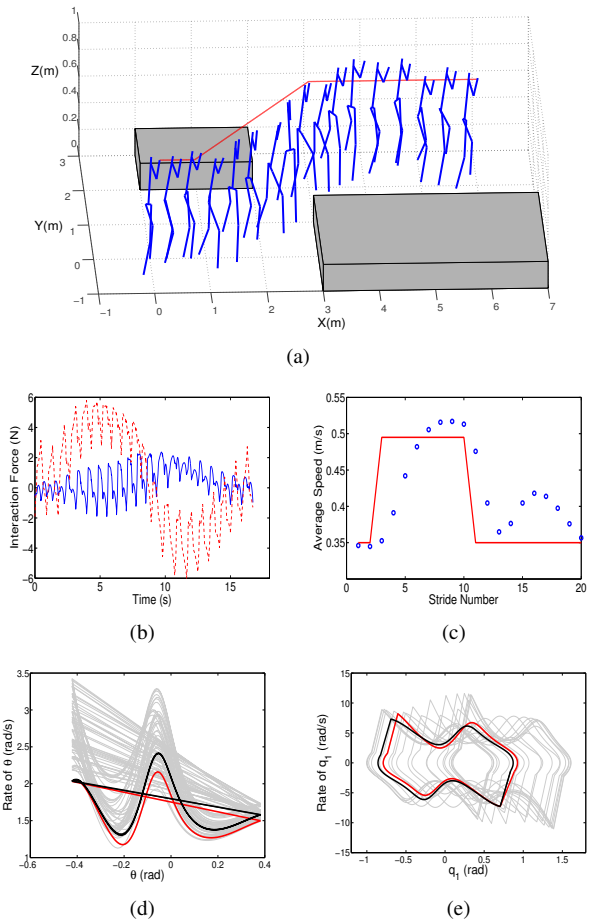

Fig. 2. (a) Biped-leader cooperation in an environment with obstacles. Intended trajectory of the leader is denoted as red line. (b) X component (blue) and Y component (dashed red) of the interaction force. (c) The intended average speed of leader (red) and average speed of biped (blue). (d) Convergence of limit cycles in terms of θ and $\dot{\theta}$. (e) Convergence of limit cycles in terms of q_1 and $\dot{q}_1$. Black is the base (unforced) limit cycle, red is the final forced limit cycle and gray correspond to transition.

As Fig. 2(d) shows, the range of values of θ remains the same during the motion; on the other hand, the rate of change $\dot{\theta}$ of θ differs. This was expected in view of the discussion in Section IV-A, which indicates that the biped in closed loop with the controller developed in Section III keeps its stride length constant as its speed and heading angle change in response to the interaction force. On the other hand, it is shown in Fig. 2(e), that the interaction force changes the evolution of both heading angle q_1 and its derivative $\dot{q}_1$.

It is natural to ask under what conditions the biped adapts its motion in response to the interaction force. Unlike the planar case [11], we cannot derive such conditions analytically in the 3D case due to the high-dimensional FHZD (19). Nevertheless, we observe in simulation that – similarly to the planar case – the biped fails when the moment of the interaction force around the stance ankle either prevents the robot to complete a step, or results in a violation of the actuation and ground contact constraints. The former occurs when the leader's speed is much lower than that of the unforced motion of the biped or when the leader makes sharp turns, while the latter failure happens when the leader's

speed is much greater than that of the unforced motion.

VI. Conclusions

This paper presented a method that unifies locomotion and manipulation controllers in a way that the motion of an underactuated 3D biped can be guided by a collaborator that physically interacts with it. The proposed approach couples impedance control on the biped's arm to appropriately handle interaction forces, with position control on the biped's legs to ensure adaptation of the locomotion system under the effect of interaction forces. It is shown that the biped adjusts its stride frequency and heading angle in response to the interaction forces. The results of this paper take a first step toward the development of controllers for cooperative object transportation tasks, in which a bipedal robot assists a human to carry an object along a path that is enforced by the human.

Appendix

Let $q_{\mathrm{z}} := (q_1, \theta, q_{10}, q_{11}, q_{12})^{\mathrm{T}}$ be the unactuated variables of the stance leg together with the variables of the arm. Then,

$$q = \tau_q \begin{bmatrix} q_{\mathrm{z}} \\ q_{\mathrm{a}} \end{bmatrix} \ , \tag{22}$$

where τ_q is a 12×12 invertible matrix. Computing $\ddot{q}$ from (22) and substituting it in (3) gives

$$D(q)\tau_q \begin{bmatrix} \ddot{q}_{\mathrm{z}} \\ \ddot{q}_{\mathrm{a}} \end{bmatrix} + H(q, \dot{q}) = \begin{bmatrix} 0_{2\times 10} \\ I_{10\times 10} \end{bmatrix} u + J_{\mathrm{E}}^{\mathrm{T}}(q) F_{\mathrm{e}}, \tag{23}$$

where $H(q, \dot{q}) := C(q, \dot{q})\dot{q} + G(q)$ and $u := (u_\ell^{\mathrm{T}}, u_{\mathrm{m}}^{\mathrm{T}})^{\mathrm{T}}$. The first two lines of (23) can be written as

$$D_{11}(q)\ddot{q}_{\mathrm{z}} + D_{12}(q)\ddot{q}_{\mathrm{a}} + H_1(q, \dot{q}) = J_{\mathrm{E},1}(q) F_{\mathrm{e}} \ , \tag{24}$$

where D_{11} is the 2×5 upper left sub-matrix of $D(q)\tau$, D_{12} is the 2×7 upper right sub-matrix of $D(q)\tau$, and H_1 and $J_{\mathrm{E},1}$ denote the first two rows of $H(q, \dot{q})$ and $J_{\mathrm{E}}^{\mathrm{T}}(q)$, respectively. Considering that on the zero dynamics (8) is identically zero, we have $q_{\mathrm{a}} = \bar{h}(\theta, \beta) := h_\ell^{\mathrm{des}}(\theta) + h_{\mathrm{c}}(\theta, \beta)$. Then, the expressions for q_{a}, $\dot{q}_{\mathrm{a}}$ and $\ddot{q}_{\mathrm{a}}$ can be obtained, and when substituted in (24) and using (22) result in

$$D_{11}(q_{\mathrm{z}})\ddot{q}_{\mathrm{z}} + D_{12}(q_{\mathrm{z}})\Big(\frac{\partial \bar{h}}{\partial \theta}\ddot{\theta} + \frac{\partial^2 \bar{h}}{\partial \theta^2}\dot{\theta}^2\Big) + H_1(q_{\mathrm{z}}, \dot{q}_{\mathrm{z}}) = J_{\mathrm{E},1}(q_{\mathrm{z}}) F_{\mathrm{e}} \ , \tag{25}$$

which are two out of the five equations needed to describe the swing phase zero dynamics. The rest of the equations result from the arm's impedance dynamics. Note that (9) depends on the arm configuration q_{m} and the monotonic variable θ, and hence is a function of q_{z}. Obtaining y_{m}, $\dot{y}_{\mathrm{m}}$ and $\ddot{y}_{\mathrm{m}}$ from (9) and substituting the results in (10) yields

$$M_{\mathrm{m}}\frac{\partial h_{\mathrm{m}}}{\partial q_{\mathrm{z}}}\ddot{q}_{\mathrm{z}} + M_{\mathrm{m}}\eta(q_{\mathrm{z}}, \dot{q}_{\mathrm{z}})\dot{q}_{\mathrm{z}} + \frac{N_{\mathrm{m}}}{\epsilon_{\mathrm{m}}}\frac{\partial h_{\mathrm{m}}}{\partial q_{\mathrm{z}}}\dot{q}_{\mathrm{z}} + \frac{K_{\mathrm{m}}}{\epsilon_{\mathrm{m}}^2}h_{\mathrm{m}} = F_{\mathrm{e}} \ , \tag{26}$$

where $\eta(q_{\mathrm{z}}, \dot{q}_{\mathrm{z}}) := \frac{d}{dt}(\frac{\partial h_{\mathrm{m}}(q_{\mathrm{z}})}{\partial q_{\mathrm{z}}})$. Combining (25) and (26), the five DOF swing phase zero dynamics can be obtained as

$$D_{\mathrm{z}}(q_{\mathrm{z}})\ddot{q}_{\mathrm{z}} + H_{\mathrm{z}}(q_{\mathrm{z}}, \dot{q}_{\mathrm{z}}) = J_{\mathrm{z}}(q_{\mathrm{z}}) F_{\mathrm{e}} \ , \tag{27}$$

where

$$D_{\mathrm{z}} := \begin{bmatrix} D_{11}(q_{\mathrm{z}}) + \begin{bmatrix} 0_{2\times 1} & D_{12}(q_{\mathrm{z}})\frac{\partial \bar{h}}{\partial \theta} & 0_{2\times 3} \end{bmatrix} \\ M_{\mathrm{m}}\frac{\partial h_{\mathrm{m}}}{\partial q_{\mathrm{z}}} \end{bmatrix} \ ,$$

$$H_{\mathrm{z}} := \begin{bmatrix} H_1(q_{\mathrm{z}}, \dot{q}_{\mathrm{z}}) + D_{12}(q_{\mathrm{z}})\frac{\partial^2 \bar{h}}{\partial \theta^2}\dot{\theta}^2 \\ M_{\mathrm{m}}\eta(q_{\mathrm{z}}, \dot{q}_{\mathrm{z}})\dot{q}_{\mathrm{z}} + \frac{N_{\mathrm{m}}}{\epsilon_{\mathrm{m}}}\frac{\partial h_{\mathrm{m}}}{\partial q_{\mathrm{z}}}\dot{q}_{\mathrm{z}} + \frac{K_{\mathrm{m}}}{\epsilon_{\mathrm{m}}^2}h_{\mathrm{m}} \end{bmatrix} \ ,$$

$$J_{\mathrm{z}}(q_{\mathrm{z}}) := \begin{bmatrix} J_{\mathrm{E},1}(q_{\mathrm{z}}) \\ I_{3\times 3} \end{bmatrix} \ .$$

References

[1] J. Dabrowski, P. Kondaxakis, and V. Kyrki, "Holding hands-guiding humanoid walking using sensorless force control," in *Proc. IEEE Int. Symp. on Robot and Human Interactive Communication*. IEEE, 2014, pp. 180–185.

[2] K. Harada, E. Yoshida, and K. Yokoi, Eds., *Motion Planning for Humanoid Robots*. Springer-Verlag, 2010.

[3] R. D. Gregg and M. W. Spong, "Reduction-based control of three-dimensional bipedal walking robots," *Int. J. of Robotics Research*, vol. 29, no. 6, pp. 680–702, May 2009.

[4] L. B. Freidovich, U. Mettin, A. S. Shiriaev, and M. W. Spong, "A passive 2-DOF walker: Hunting for gaits using virtual holonomic constraints," *IEEE Transactions on Robotics*, vol. 25, no. 5, pp. 1202–1208, October 2009.

[5] E. R. Westervelt, J. W. Grizzle, C. Chevallereau, J. H. Choi, and B. Morris, *Feedback Control of Dynamic Bipedal Robot Locomotion*. Boca Raton, FL: CRC Press, 2007.

[6] C. Chevallereau, J. W. Grizzle, and C.-L. Shih, "Asymptotically stable walking of a five-link underactuated 3-D bipedal robot," *IEEE Transactions on Robotics*, vol. 25, no. 1, pp. 37–50, 2009.

[7] Q. Nguyen and K. Sreenath, "Optimal robust control for bipedal robots through control lyapunov function based quadratic programs," in *Proc. of Robotics: Science and Systems*, 2015.

[8] K. A. Hamed and J. W. Grizzle, "Event-based stabilization of periodic orbits for underactuated 3-D bipedal robots with left-right symmetry," *IEEE Transactions on Robotics*, vol. 30, no. 2, pp. 365–381, 2014.

[9] C. O. Saglam and K. Byl, "Robust policies via meshing for metastable rough terrain walking," in *Proc. of Robotics: Science and Systems*, 2014.

[10] A. D. Ames and M. Powell, "Towards the unification of locomotion and manipulation through control lyapunov functions and quadratic programs," in *Control of Cyber-Physical Systems, Lecture Notes in Control and Information Sciences*. Springer, 2013, pp. 219–240.

[11] M. S. Motahar, S. Veer, J. Huang, and I. Poulakakis, "Integrating dynamic walking and arm impedance control for cooperative transportation," in *Proc. of IEEE/RSJ Int. Conf. on Intelligent Robots and Systems*, Hamburg, Germany, September 2015.

[12] S. Veer, M. S. Motahar, and I. Poulakakis, "On the adaptation of dynamic walking to persistent external forcing using hybrid zero dynamics control," in *Proc. of IEEE/RSJ Int. Conf. on Intelligent Robots and Systems*, Hamburg, September 2015, pp. 997–1003.

[13] ——, "Local input-to-state stability of dynamic walking under persistent external excitation using hybrid zero dynamics," in *Proc. of the American Control Conf.*, Boston, July 2016, pp. 4801–4806.

[14] C.-L. Shih, J. Grizzle, and C. Chevallereau, "From stable walking to steering of a 3D bipedal robot with passive point feet," *Robotica*, vol. 30, no. 7, pp. 1119–1130, 2012.

[15] R. D. Gregg, A. K. Tilton, S. Candido, T. Bretl, and M. W. Spong, "Control and planning of 3-D dynamic walking with asymptotically stable gait primitives," *Transactions on Robotics*, vol. 28, no. 6, pp. 1415–1423, 2012.

[16] M. S. Motahar, S. Veer, and I. Poulakakis, "Composing limit cycles for motion planning of 3D bipedal walkers," in *Proc. of IEEE Conf. on Decision and Control*, Las Vegas, December 2016.

[17] S. Veer, M. S. Motahar, and I. Poulakakis, "Almost driftless navigation of 3D limit-cycle walking bipeds," in *Proc. of IEEE/RSJ Int. Conf. on Intelligent Robots and Systems*, 2017.

[18] F. Popescu, J. M. Hidler, and W. Z. Rymer, "Elbow impedance during goal-directed movements," *Experimental brain research*, vol. 152, no. 1, pp. 17–28, 2003.